Hybrid Cable-Thruster Actuated Underwater Vehicle Manipulator Systems: A Study on Force Capabilities

Gamal El-Ghazaly, Marc Gouttefarde, Vincent Creuze

Hybrid Cable-Thruster Actuated Underwater Vehicle-Manipulator Systems: A Study on Force Capabilities

Gamal El-Ghazaly, Marc Gouttefarde, and Vincent Creuze

***Abstract*—Traditional underwater vehicle-manipulator systems (UVMS) consist mainly of an underwater vehicle on which a manipulator is mounted. In addition to the vehicle thrusters, this paper proposes to use cables to actuate UVMSs. The main goal of this extra source of actuation is to enhance UVMS work capabilities. Similarly to cable-driven parallel robots, the cables are attached to the UVMS and a set of fixed winches permit the control of the cable lengths or tensions. We refer to this new system as a hybrid cable-thruster (HCT)-actuated UVMS. Based on the kinematic and dynamic model of HCT-actuated UVMSs, this paper focuses on the determination of the available set of end-effector forces in a suitable mathematical representation. An illustrative simple planar example of HCT-actuated UVMS is also presented.**

I. Introduction

Underwater robotic platforms have been found very convenient in a wide range of field operations for marine applications due to the hazardous and hostile nature of underwater environments [1]. Among the prominent application domains of underwater robotic platforms are offshore industries, military applications, and scientific purposes. For those application domains, underwater robotics are supposed to target various operational tasks. Survey missions, inspection and interventions on subsea installations, observations, salvage, recovery/retrieval and communications are among the broad range of operational tasks that could be achieved by underwater robotic systems [2], [3], [4]. Underwater vehicles equipped with manipulators are called underwater vehicle-manipulator systems (UVMS). One key challenge related to UVMSs is to enhance their work capabilities. Indeed, it may be desired to perform field operations such as handling large and versatile tools (grippers, drillers, probes, etc.), handling heavy payloads, and interacting more strongly and dexterously with the environment [1], [2]. Interventions on subsea installations and offshore platforms in the Oil and Gas industry need such capabilities [5]. In fact, UVMS work capabilities are in direct relation to the vehicle thruster capabilities. For instance, handling a heavy payload would require a larger number of thrusters and/or more powerful ones, which in turn, increase the cost, size, weight, and design complexity of the system. From this perspective, improving UVMS work capabilities should allow underwater field operation tasks that existing UVMS can hardly accomplish.

G. El-Ghazaly, M. Gouttefarde, and V. Creuze are with the Laboratoire d'Informatique, de Robotique et de Microélectronique de Montpellier (LIRMM-CNRS-Université de Montpellier), 161 Rue Ada, 34095, Montpellier Cedex 05, France {gamal.elghazaly, marc.gouttefarde, vincent.creuze}@lirmm.fr

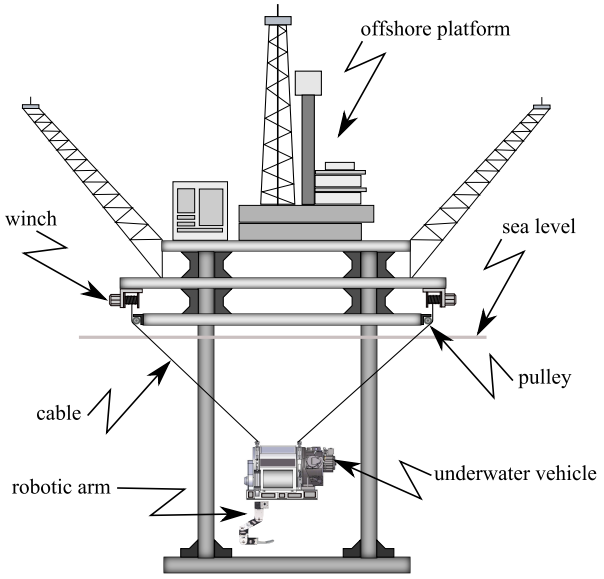

Fig. 1: An HCT-actuated UVMS installed on an offshore platform

In this paper, we introduce a novel concept for an underwater robotic platform, as illustrated in Fig. 1. The concept is inspired by cable-driven parallel robots (CDPR) which consist of a moving platform connected to a fixed base through a set of cables. The cable lengths or the cable tensions are controlled by a set of winches which are generally attached to the fixed base (see [6] and [7] for the basic principles). CDPRs allow motion and force transmission from the fixed base to the moving platform over long distances. Moreover, the cable lengths can be used to determine, or at least, estimate the position and orientation of the moving platform, e.g. [8]. Therefore, CDPRs are excellent candidates for applications that require very large workspaces at a relatively low cost. Besides, CDPRs can be designed to handle heavy payloads [9]. Our main objective is to take advantage of the aforementioned favorable features of CDPRs for underwater applications. In the proposed solution, in addition to the thrusters, cables are employed as a supplementary source of actuation to the underwater vehicle. When powerful cable winches are used (e.g., winches located on an oil rig), this extra actuation via cables should significantly increase the lifting capabilities of

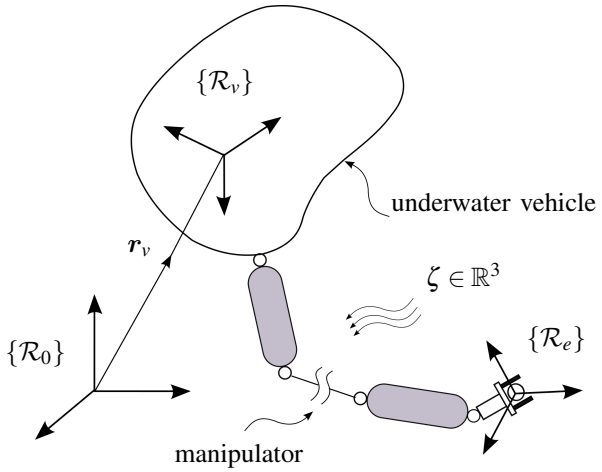

Fig. 2: A schematic representation of an UVMS

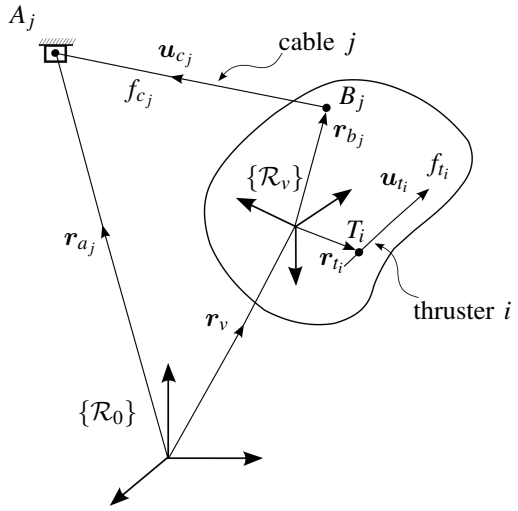

Fig. 3: Hybrid cable-thruster actuation model

an UVMS. Throughout this paper, we refer to the proposed system as a *Hybrid Cable-Thruster* (HCT)-actuated UVMS. For the sake of illustration, Fig. 1 shows a typical arrangement of an HCT-actuated UVMS attached to an offshore platform wherein the cable winches are fixed to the offshore platform structure and the cables are attached to the UVMS. Among the many challenges related to the design and control of HCT-actuated UVMS, the technical contribution of this paper is the characterization of their force capabilities.

This paper is organized as follows: Section II summarizes the kinematic and dynamic modeling of the proposed HCT-actuated UVMS. Based on this modeling, Section III describes three relevant available force sets. Section IV is mostly dedicated to the determination of the available end-effector force set, where the latter is represented in a form that eases its use to check whether or not a given desired force is feasible. Section V presents an illustrative planar example of an HCT-actuated UVMS which is equipped with a 2-DOF manipulator and actuated by four thrusters and two cables. Section VI concludes the paper.

II. HCT-Actuated UVMS: Description and Modeling

An UVMS as shown in Fig. 2 is composed of n_m+1 rigid links. The first link represents the vehicle and the remaining links represent an n_m-DOFs serial manipulator attached to the vehicle. Consider a fixed reference frame $\{\mathcal{R}_0\}$ attached to a support structure which is assumed to be inertial. The frames $\{\mathcal{R}_v\}$ and $\{\mathcal{R}_e\}$ are attached to the vehicle and the end-effector of the manipulator, respectively. We define the configuration of the UVMS as

$$\boldsymbol{q} = \begin{pmatrix} \boldsymbol{q}_v \\ \boldsymbol{q}_m \end{pmatrix} \in \mathcal{CS} \tag{1}$$

where $\boldsymbol{q}_v \in SE(3)$ and $\boldsymbol{q}_m \in \mathbb{R}^{n_m}$ are the generalized coordinates of the vehicle and the manipulator, respectively. For instance, a minimal representation for the configuration of the vehicle is the position $\boldsymbol{r}_v = \left(x_v, y_v, z_v\right)^T$ and Euler angles $\theta_v = \left(\phi_v, \theta_v, \psi_v\right)^T$ as a representation of the orientation of $\{\mathcal{R}_v\}$ with respect to $\{\mathcal{R}_0\}$. Thus, one may have $\boldsymbol{q}_v = \left(\boldsymbol{r}_v^T, \theta_v^T\right)^T \in \mathbb{R}^6$, in which case, the dimension of the configuration space of the UVMS is $n_q = \dim(\mathcal{CS}) = 6+n_m$. The dynamic model of an UVMS in the configuration space may be expressed as follows

$$\boldsymbol{M}(\boldsymbol{q})\ddot{\boldsymbol{q}} + \boldsymbol{C}(\boldsymbol{q},\dot{\boldsymbol{q}})\dot{\boldsymbol{q}} + \boldsymbol{D}(\boldsymbol{q},\dot{\boldsymbol{q}},\zeta) + \boldsymbol{Q}(\boldsymbol{q}) + \boldsymbol{J}_e^T(\boldsymbol{q})\boldsymbol{f}_e = \boldsymbol{f}_q \tag{2}$$

where $\boldsymbol{M}(\boldsymbol{q})$ is a square positive definite symmetric matrix representing rigid body inertia and the added mass. The matrix $\boldsymbol{C}(\boldsymbol{q},\dot{\boldsymbol{q}})$ represents the corresponding Coriolis and centrifugal effects. The vector $\boldsymbol{D}(\boldsymbol{q},\dot{\boldsymbol{q}},\zeta)$ represents the damping and drag forces, where $\zeta \in \mathbb{R}^3$ is the sea current velocity. The vector $\boldsymbol{Q}(\boldsymbol{q})$ represents the restoring forces due to gravity and buoyancy. The vector $\boldsymbol{f}_e \in \mathbb{R}^{n_e}$ is the force that the system can apply to the environment by its end-effector. The vector $\boldsymbol{f}_q \in \mathbb{R}^{n_q}$ represents the generalized forces that act on the configuration space of the UVMS. The end-effector force $\boldsymbol{f}_e$ is projected to a generalized force in the configuration space via the transpose of the Jacobian matrix $\boldsymbol{J}_e(\boldsymbol{q})$. This matrix also maps the generalized velocity $\dot{\boldsymbol{q}}$ to the spatial velocity of the end-effector $\dot{\boldsymbol{x}}_e \in \mathbb{R}^{n_e}$ as

$$\dot{\boldsymbol{x}}_e = \boldsymbol{J}_e(\boldsymbol{q})\dot{\boldsymbol{q}} \tag{3}$$

Since $n_e \leq 6$ and $n_q = 6+n_m$, $n_q > n_e$ which implies that the UVMS is kinematically redundant [10]. More details on the UVMS modeling described above can be found in [11], [12], [13]. Unlike classical UVMSs for which the vehicle is actuated only by n_t thrusters, n_c cables (actuated by winches as in CDPRs) are used in addition to the thrusters which results in a hybrid actuation of the vehicle. For the sake of simplicity, thrusters are assumed to be *pure force generators* (i.e. their propellers' induced torques are neglected). For each thruster i, $i = 1, 2, \ldots, n_t$, f_{t_i} and $\boldsymbol{r}_{t_i}$ denote respectively, the thrust force and a position vector of a point on the thruster line of action with direction defined by the unit vector $\boldsymbol{u}_{t_i}$ (see Fig. 3). The additional vehicle actuation via n_c cables is defined as follows. For each cable j, $j = 1, 2, \ldots, n_c$, points A_j and B_j

are the fixed base and vehicle cable attachments, respectively. $\boldsymbol{r}_{a_j}$ and $\boldsymbol{r}_{b_j}$ are the position vectors of A_j and B_j expressed in frames $\{\mathcal{R}_0\}$ and $\{\mathcal{R}_v\}$, respectively. We also denote $\boldsymbol{u}_{c_j}$ and f_{c_j} the unit vector along the cable direction B_jA_j and the cable tension, respectively (see Fig. 3). For simplicity, the cables are assumed to have negligible mass and elasticity. They are considered as a *unilateral force generators*. Similar to the definition of the generalized coordinates, we can define the vector of generalized forces as $\boldsymbol{f}_q = \left(\boldsymbol{f}_v^T, \boldsymbol{f}_m^T\right)^T$, where $\boldsymbol{f}_v$ represents the generalized forces acting on the vehicle and $\boldsymbol{f}_m$ are the joint torques of the manipulator. The generalized vehicle force $\boldsymbol{f}_v$ is expressed as

$$\boldsymbol{f}_v = \boldsymbol{J}_v^T(\boldsymbol{q})\Big(\boldsymbol{J}_t^T\boldsymbol{f}_t + \boldsymbol{J}_c^T(\boldsymbol{q})\boldsymbol{f}_c\Big) \tag{4}$$

where $\boldsymbol{J}_v$ is a spatial transformation matrix that maps the generalized velocities of the vehicle $\boldsymbol{q}_v$ into the spatial velocity $\boldsymbol{v}_v = \left(v_v^T\ \boldsymbol{\omega}_v^T\right)^T$, i.e. the velocity of the vehicle expressed in $\{\mathcal{R}_v\}$. The matrix $\boldsymbol{J}_t^T$ is called *thruster configuration matrix* [14], [15], [16]. It maps the thruster forces $\boldsymbol{f}_t = \left[f_{t_1}, f_{t_2}, \ldots, f_{n_t}\right]^T$ into a wrench expressed in $\{\mathcal{R}_v\}$. The matrix $\boldsymbol{J}_c^T(\boldsymbol{q})$ maps the cable tensions $\boldsymbol{f}_c = \left[f_{c_1}, f_{c_2}, \ldots, f_{n_c}\right]^T$ into a wrench expressed in $\{\mathcal{R}_v\}$ and is called *cable wrench matrix* [17]. The matrices $\boldsymbol{J}_t^T$ and $\boldsymbol{J}_c^T(\boldsymbol{q})$ can be expressed, respectively, as follows

$$\boldsymbol{J}_t^T = \begin{bmatrix} \boldsymbol{u}_{t_1} & \boldsymbol{u}_{t_2} & \ldots & \boldsymbol{u}_{t_{n_t}} \\ \boldsymbol{r}_{t_1}\times\boldsymbol{u}_{t_1} & \boldsymbol{r}_{t_2}\times\boldsymbol{u}_{t_2} & \ldots & \boldsymbol{r}_{t_{n_t}}\times\boldsymbol{u}_{t_{n_t}} \end{bmatrix}, \tag{5}$$

$$\boldsymbol{J}_c^T = \begin{bmatrix} \boldsymbol{u}_{c_1} & \boldsymbol{u}_{c_2} & \ldots & \boldsymbol{u}_{c_{n_c}} \\ \boldsymbol{r}_{c_1}\times\boldsymbol{u}_{c_1} & \boldsymbol{r}_{c_2}\times\boldsymbol{u}_{c_2} & \ldots & \boldsymbol{r}_{c_{n_c}}\times\boldsymbol{u}_{c_{n_c}} \end{bmatrix} \tag{6}$$

Note that the unit vectors $\boldsymbol{u}_{t_i}$ and $\boldsymbol{u}_{c_j}$ (see Fig. 3) are defined with respect to $\{\mathcal{R}_v\}$. The vector $\boldsymbol{u}_{t_i}$ is constant in $\{\mathcal{R}_v\}$ whereas $\boldsymbol{u}_{c_j}$ depends on the vehicle configuration $\boldsymbol{q}_v$. According to the capabilities of the motors actuating the thrusters, the generated propeller forces f_{t_i} is limited by a lower bound $f_{t_i}^{min}$ and an upper bound $f_{t_i}^{max}$. Since cables can provide only tensile forces, the cable actuation forces f_{c_i} have non-negative minimum value $f_{c_i}^{min}$ and maximum value $f_{c_i}^{max}$. The lower limit $f_{c_i}^{min}$ is ideally zero. However, in practice, it must be set to a given strictly positive value to maintain the cables in tension [18]. Using (4), the overall actuation forces acting on the generalized coordinates can be written in a compact form as:

$$\boldsymbol{f}_q = \boldsymbol{J}_a^T(\boldsymbol{q})\boldsymbol{f}_a \tag{7}$$

where $\boldsymbol{f}_a = \left(\boldsymbol{f}_t^T, \boldsymbol{f}_c^T, \boldsymbol{f}_m^T\right)^T$ is the vector of all actuation forces for the HCT-actuated UVMS with dimension $n_a = n_t + n_c + n_m$ and the *actuation matrix* $\boldsymbol{J}_a^T(\boldsymbol{q})$ is an $n_q \times n_a$ given by

$$\boldsymbol{J}_a^T(\boldsymbol{q}) = \begin{bmatrix} \boldsymbol{J}_v^T\boldsymbol{J}_t^T & \boldsymbol{J}_v^T\boldsymbol{J}_c^T & \boldsymbol{0} \\ \boldsymbol{0} & \boldsymbol{0} & \boldsymbol{I} \end{bmatrix} \tag{8}$$

where $\boldsymbol{0}$ and $\boldsymbol{I}$ are null and identity matrices with appropriate dimensions. Equations (2) and (7) represent the overall dynamic model of an HCT-actuated UVMS. In case of a vehicle fully-actuated by thrusters, adding cable actuation leads to actuation redundancy. If no cables are used, the model is the same except that the additional cable forces are removed. The columns in $\boldsymbol{J}_a^T(\boldsymbol{q})$ corresponding to $\boldsymbol{f}_c$ are removed, i.e. $\boldsymbol{f}_a = \left(\boldsymbol{f}_t^T, \boldsymbol{f}_m^T\right)^T$ and

$$\boldsymbol{J}_a^T(\boldsymbol{q}) = \begin{bmatrix} \boldsymbol{J}_v^T\boldsymbol{J}_t^T & \boldsymbol{0} \\ \boldsymbol{0} & \boldsymbol{I} \end{bmatrix} \tag{9}$$

III. Characterization of HCT-Actuated UVMS Force Spaces

Based on the UVMS model presented in Section II, the present section deals with the characterization of the available end-effector force set. This force set describes the ability of an HCT-actuated UVMS to apply forces to the environment at its end-effector. Therefore, it determines whether or not the robotic system can meet the force requirements of a given task. Once the force set available at the end-effector is determined, one may check the inclusion of the required task forces in the available force set. Actually, such capabilities are related to the lower and upper bounds on the components of the vector of actuation forces $\boldsymbol{f}_a$. To understand the relation between the available end-effector force set and the bounds on $\boldsymbol{f}_a$, let us consider the overall UVMS model described by (2) and (7). First, Eq. (7) implies that the generalized coordinates $\boldsymbol{q}$ are not *directly* actuated as in serial manipulators, where the generalized coordinates are usually selected to be the actuated joints. In fact, the actuation matrix $\boldsymbol{J}_a^T(\boldsymbol{q})$ is used as a mapping from the actuation space to the space of generalized forces. The generalized forces $\boldsymbol{f}_q$ should concurrently (a) produce the required end-effector forces $\boldsymbol{f}_e$ (via the fifth term of (2)), (b) compensate the gravity and buoyancy forces $\boldsymbol{Q}(\boldsymbol{q})$, (c) compensate for drag and damping forces $\boldsymbol{D}(\boldsymbol{q},\dot{\boldsymbol{q}},\boldsymbol{\zeta})$, and (d) move the UVMS with velocity $\dot{\boldsymbol{q}}$ and acceleration $\ddot{\boldsymbol{q}}$. Since this paper focuses on the characterization the available end-effector forces, (2) is written in the following compact form

$$\boldsymbol{h}(\boldsymbol{q},\dot{\boldsymbol{q}},\ddot{\boldsymbol{q}},\boldsymbol{\zeta}) + \boldsymbol{J}_e^T(\boldsymbol{q})\boldsymbol{f}_e = \boldsymbol{f}_q \tag{10}$$

where, $\boldsymbol{h} = \boldsymbol{M}(\boldsymbol{q})\ddot{\boldsymbol{q}} + \boldsymbol{C}(\boldsymbol{q},\dot{\boldsymbol{q}})\dot{\boldsymbol{q}} + \boldsymbol{D}(\boldsymbol{q},\dot{\boldsymbol{q}},\zeta) + \boldsymbol{Q}(\boldsymbol{q})$ At static equilibrium, $\boldsymbol{h}$ is reduced to gravity, buoyancy and sea current damping.

According to (7) and (10), there are three force spaces relevant to the problem of characterizing force capabilities of an UVMS. These force spaces are associated with actuation forces $\boldsymbol{f}_a \in \mathbb{R}^{n_a}$, generalized forces forces $\boldsymbol{f}_q \in \mathbb{R}^{n_q}$, and end-effector forces $\boldsymbol{f}_e \in \mathbb{R}^{n_e}$. The lower and upper bounds on $\boldsymbol{f}_a$ define the bounded set of the available actuation forces in the actuation space. Consequently, the available force sets in generalized coordinates and at the end-effector are also bounded. Let us denote $\mathcal{F}_a$, $\mathcal{F}_q$, and $\mathcal{F}_e$ the available force sets in the actuation space, generalized coordinates, and at the end-effector, respectively. If $\boldsymbol{f}_a^m = [f_{a_1}^m, f_{a_2}^m, \ldots, f_{a_{n_a}}^m]^T$ and $\boldsymbol{f}_a^M = [f_{a_1}^M, f_{a_2}^M, \ldots, f_{a_{n_a}}^M]^T$ are the vectors of lower and upper bounds on the components of $\boldsymbol{f}_a$, respectively, $\mathcal{F}_a$ is the following hypercube

$$\mathcal{F}_a = \left\{\boldsymbol{f}_a \,|\, f_{a_i} \in [f_{a_i}^m, f_{a_i}^M], \forall i, 1 \le i \le n_a\right\} \tag{11}$$

The set of available generalized-coordinate forces $\mathcal{F}_q$ can then be expressed using (7) as

$$\mathcal{F}_q = \left\{\boldsymbol{f}_q \,|\, \boldsymbol{f}_q = \boldsymbol{J}_a^T\boldsymbol{f}_a,\ \boldsymbol{f}_a \in \mathcal{F}_a\right\} \tag{12}$$

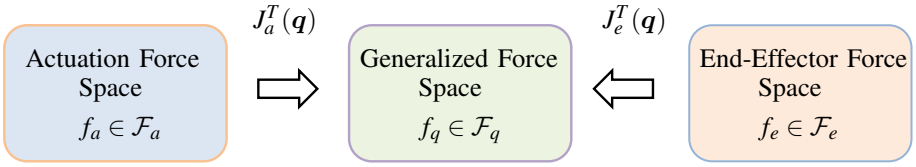

Fig. 4: An illustration of the mappings between the available force sets in the actuation space $\mathcal{F}_a \subseteq \mathbb{R}^{n_a}$, in generalized coordinates $\mathcal{F}_q \subseteq \mathbb{R}^{n_q}$, and at the end-effector $\mathcal{F}_e \subseteq \mathbb{R}^{n_e}$.

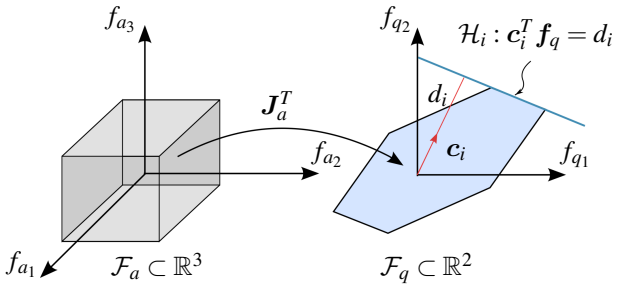

Fig. 5: Mapping of $\mathcal{F}_a$ to $\mathcal{F}_q$ with n_a = dim($\mathcal{F}_a$) = 3 and n_q = dim($\mathcal{F}_q$) = 2.

In a similar manner, the set of available end-effector forces $\mathcal{F}_e$ is

$$\mathcal{F}_e = \{ f_e \,|\, J_e^T f_e + h = f_q,\ f_q \in \mathcal{F}_q \} \tag{13}$$

The majority of UVMSs are equipped with thrusters such that the matrix J_t^T is full rank. As a matter of fact, with the extra cable actuation, the number of actuators n_a is greater than the number n_q of generalized coordinates in a minimum representation ($n_a > n_q$). This implies that the HCT-actuated UVMS has actuation redundancy. Additionally, it is also kinematically redundant since the dimension of the end-effector space n_e is smaller than n_q ($n_q < n_e$). On the one hand, for manipulators having only actuation redundancy (for example, when the robotic arm is removed from the UVMS), $n_e = n_q$ and the set of available forces at the end-effector $\mathcal{F}_e$ is explicitly given by

$$\mathcal{F}_e = \{ f_e \,|\, f_e = J_e^{-T} J_a^T f_a - J_e^{-T} h,\ f_a \in \mathcal{F}_a \} \tag{14}$$

On the other hand, for manipulators with only kinematic redundancy (for example, when $n_c = 0$ and the vehicle is fully actuated by 6 thrusters whose generated forces are linearly independent), we have $n_q = n_a$ and $\mathcal{F}_e$ is characterized by

$$\mathcal{F}_e = \{ f_e \,|\, J_a^{-T} J_e^T f_e + J_a^{-T} h = f_a,\ f_a \in \mathcal{F}_a \} \tag{15}$$

IV. Redundancy and Available Force Sets of HCT-Actuated UVMSs

The first objective of this section is to determine the available end-effector force set $\mathcal{F}_e$ for the proposed HCT-actuated UVMSs. In order to verify if a given desired end-effector force f_e^d can be exerted, i.e. to verify if $f_e^d \in \mathcal{F}_e$, $\mathcal{F}_e$ should be described by an appropriate representation. We will also present a method to quantify the force capability along the direction of the desired force to be exerted by the end-effector of the robot. These goals can be achieved by having $\mathcal{F}_e$ in the so-called $\mathcal{H}$-representation, i.e., as the intersection of a finite set of halfspaces. Since $\mathcal{F}_e$ can hardly be determined directly from $\mathcal{F}_a$, we determine $\mathcal{F}_q$ from $\mathcal{F}_a$ via (12) and then determine $\mathcal{F}_e$ from $\mathcal{F}_q$ via (13). Fig. 4 illustrates the mappings between the different force spaces relevant to our problem. We can determine $\mathcal{F}_q$ in two different ways. The first method is to map the vertices of $\mathcal{F}_a$ via J_a^T and a convex hull algorithm is then applied to compute the vertices of $\mathcal{F}_q$ [19]. However, the determination of the desired $\mathcal{H}$-representation of $\mathcal{F}_e$ from the knowledge of the vertices of $\mathcal{F}_a$ is not straightforward. Alternatively, the so-called hyperplane shifting method introduced in [20] or its modified version [21] can be to have $\mathcal{F}_q$ in $\mathcal{H}$-representation. As shown in Fig. 5, $\mathcal{F}_q$ is then described as the intersection of a set of halfspaces $\mathcal{H}_i^- = \{ f_q \,|\, c_i^T f_q \leq d_i \}$, $i = 1, 2, \ldots, p$, where p is the number of halfspaces, $c_i \in \mathbb{R}^{n_q}$, and $d_i \in \mathbb{R}$. In other words, $\mathcal{F}_q$ is given by

$$\mathcal{F}_q = \{ f_q \,|\, C_q^T f_q \leq d_q \}, \tag{16}$$

where $C_q = [c_1, c_2, \ldots, c_p]$, and $d_q = [d_1, d_2, \ldots, d_p]$. The $\mathcal{H}$-representation of $\mathcal{F}_e$ must now be determined from the $\mathcal{H}$-representation of $\mathcal{F}_q$ in (16). A similar problem of determining $\mathcal{F}_e$ from $\mathcal{F}_q$ has been addressed for kinematically redundant serial manipulators in [22] where $\mathcal{F}_q$ is a hypercube. This method may be extended to the more general case dealt with in the present paper. However, the $\mathcal{H}$-representation of $\mathcal{F}_e$ can be obtained more straightforwardly by substituting the expression of f_q in (10) into (16) to get

$$\mathcal{F}_e = \{ f_e \,|\, C_e^T f_e \leq d_e \}, \tag{17}$$

where, $C_e = J_e C_q$ and $d_e = d_q - C_q^T h$. From (17), one can easily verify if a desired force f_e^d can be generated by checking the validity of $C_e^T f_e^d \leq d_e$.

The second goal of this section is to verify if the HCT-actuated UVMS meets the force requirements of a given task along a configuration trajectory $\mathcal{Q}$. We present a simple method to quantify to what extent the system is capable of exerting a force along the direction of a desired force f_e^d. Let us assume that $\forall q \in \mathcal{Q}$, the manipulator must exert a desired end-effector force $f_e^d(q)$. This desired force could be written as $f_e^d = \alpha_o s$, where $\alpha_o = \| f_e^d \|$ represents the strength of f_e^d along the unit vector s[1]. To ensure that the system is capable

[1]Since f_e is a spatial force vector, i.e., a wrench, the value of α_o does not have a proper physical unit; Nonetheless, in the sake of simplicity, it is used here to quantify the strength of f_e^d.

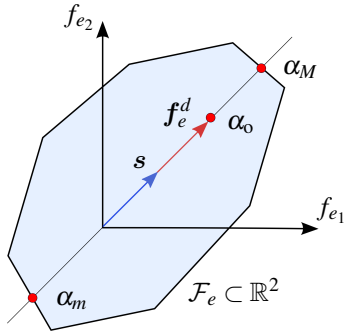

Fig. 6: Definitions of α_o, α_m, and α_M

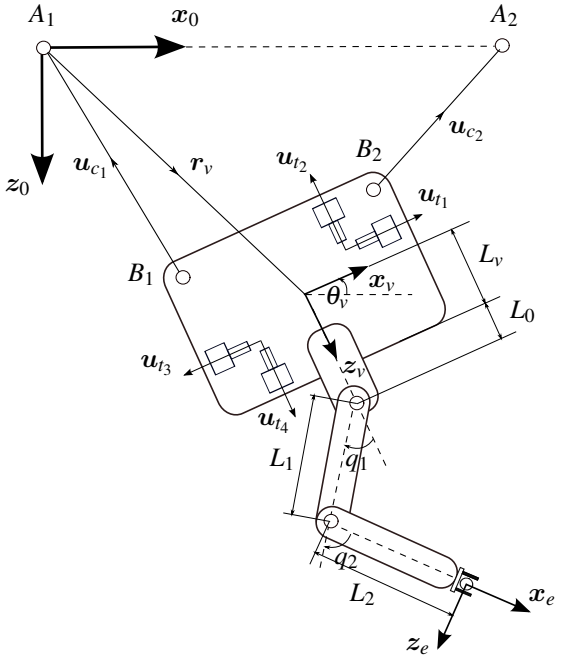

Fig. 7: An UVMS in vertical plane

of exerting a force along s, we have to determine the range of $\alpha = [\alpha_m, \alpha_M]$ such that $f_e = \alpha s \in \mathcal{F}_e$. By means of the $\mathcal{H}$-representation of $\mathcal{F}_e$ in (17), α_m and α_M can be easily determined from the intersection of s with $\mathcal{F}_e$ (see Fig. 6) as

$$\alpha_m = \max_{i:[C_e^T s]_i<0} \frac{[d_e]_i}{[C_e^T s]_i}, \quad \alpha_M = \min_{i:[C_e^T s]_i>0} \frac{[d_e]_i}{[C_e^T s]_i} \tag{18}$$

where $[a]_i$ represents the i-th component of the vector a. Since $\alpha_o \geq 0$ by definition, $[\alpha_m, \alpha_M] \cap \mathbb{R}^+$ must not be empty if the robot is to be able to exert a force along the desired direction. If $\alpha_o \in [\alpha_m, \alpha_M]$, the desired force can be exerted and $\alpha_M - \alpha_o$ quantifies the ability to exert larger forces along the same direction.

V. Case Study: Planar HCT-Actuated UVMS

In this section, we use the method presented in Section IV to show that actuation by cables can significantly improve the force capabilities of UVMSs. For the sake of simplicity, a planar HCT-actuated UVMS is considered. The planar UVMS, as shown in Fig. 7, is composed of a vehicle with generalized coordinates $q_v = [x_v, z_v, \theta_v]^T$. The vehicle is equipped with a

TABLE I: Parameters of the Thrusters

thruster	r_t $[m]$	u_t $[m]$	f_t^m $[N]$	f_t^M $[N]$
1	$[0.25, -0.25]^T$	$[1, 0]^T$	-75	75
2	$[0.25, -0.25]^T$	$[0, -1]^T$	-75	75
3	$[-0.25, 0.25]^T$	$[-1, 0]^T$	-75	75
4	$[-0.25, 0.25]^T$	$[0, 1]^T$	-75	75

TABLE II: Parameters of the Cables

cable	r_a $[m]$	r_b $[m]$	f_c^m $[N]$	f_c^M $[N]$
1	$[0, 0,]^T$	$[-0.5, -0.5]^T$	20	1000
2	$[50, 0]^T$	$[0.5, -0.5]^T$	20	1000

2-DOF manipulator, i.e. $n_m = 2$, with generalized coordinates $q_m = [q_1, q_2]^T$. Hence, the configuration space of the UVMS has a dimension $n_q = 5$. The vehicle has a hybrid actuation system of four thrusters and two cables, i.e. $n_t = 4$ and $n_c = 2$. The coordinates of the end-effector position are $x_e = [x_e, z_e]^T$, which means that $n_e = 2$. Table I shows the position vectors r_t and the direction unit vectors u_t of the four thrusters, as well as their minimum and maximum thrust forces, f_t^m and f_t^M. Table II shows the position vectors r_a and r_b of the attachment points of the two cables, as well as their minimum and maximum tensions, f_c^m and f_c^M. The minimum and maximum joint torques f_m^m and f_m^M of the manipulator are given in Table III. The HCT-actuated UVMS has a total number of $n_a = 8$ actuators, then its degree of actuation redundancy is $n_a - n_q = 3$. For a cable-free version, the degree of actuation redundancy would be $n_a - n_q = 1$. The system is also kinematically redundant and its degree of kinematic redundancy is $n_q - n_e = 3$. The parameters of the individual rigid bodies of the UVMS are given in Table IV and are the same as in [11]. The sea current velocity is assumed, for simplicity, to be constant $\zeta = [0.25, 0]^T\ m/s$. The water density is $\rho = 1024\,kg/m^3$ and the gravity acceleration is $g = 9.81\,m/s^2$. In this example, the desired path of the end-effector is a $1\,m$ radius circle (see Fig. 8a). The path in configuration space $\mathcal{Q}$, shown in Fig. 8b and Fig. 8c, is chosen such that it has a minimum norm solution of its differential kinematics, i.e., $\delta q = J_e^+(q)\delta x_e$. For simplicity, the desired force to be exerted by the end-effector along $\mathcal{Q}$ is assumed to be a constant value $f_e^d(q) = [0, -150]^T\,\mathrm{N}$ for all $q \in \mathcal{Q}$. This means that $\alpha_o = 150\mathrm{N}$ and $s = [0, -1]^T$. For each $q \in \mathcal{Q}$, the available end-effector force set is determined in $\mathcal{H}$-representation as described in Section IV for both HCT-actuated UVMS and its cable-free version. The limits of the feasible set $\mathcal{F}_e$ along s, i.e., α_m and α_M is determined via (18). Fig. 9a and Fig. 9b show the evolution of α_m and α_M along the

TABLE III: Torque Limits of the Manipulator

Joint	f_m^m $[N.m]$	f_m^M $[N.m]$
1	-171.2	171.2
2	-73.3	73.3

TABLE IV: UVMS Body Parameters: body length L, width W, mass M, center of mass COM, volume V, center of buoyancy COB, and damping parameters

UVMS body	L $[m]$	W $[m]$	M $[Kg]$	COM $[m]$	V $[m^3]$	COB $[m]$	diag$(X_{u\|u\|}, Z_{w\|w\|}, M_{q\|q\|})$
Vehicle	0.347	1.0	145	$[0.035, 0]^T$	0.1534	$[-0.005, 0]^T$	diag$(-76.8088, -56.3654, -76.7628)$
Link 0	0.315	0.2	17.82	$[0.1825, 0]^T$	0.0.013609	$[0.18055, 0]^T$	diag$(-22.567, -29.4246, -0.7299)$
Link 1	0.450	0.15	9.86	$[0.30, 0]^T$	0.0.007128	$[0.3273, 0]^T$	diag$(-9.757, -29.934, -1.3635)$
Link 2	0.500	0.10	6.28	$[0.3243, 0]^T$	0.0.004547	$[0.32142, 0]^T$	diag$(-5.5542, -22.579, -1.4112)$

path for the HCT-actuated UVMS and its cable-free version, respectively. It can be easily seen that $[\alpha_m, \alpha_M] \cap \mathbb{R}^+ \neq \emptyset$ in both cases. However, the HCT-actuated UVMS is capabable of exerting larger forces along s compared to the case of UVMS without cable actuation. Indeed, the maximum force exerted by the UVMS along the positive direction of s is at least 980 N with cable actuation while it is only 57 N without cable actuation. In the opposite direction of s, the minimum exerted force is almost the same for both actuation cases. This is due to the unilateral nature of the cable tensions (cables can "pull" but cannot "push"). This planar example illustrates the improved force capability of the HCT-actuated UVMS with respect to the conventional UVMS. This simple example has been selected for illustration purposes. The framework introduced in this paper can be applied to more complicated UVMSs.

VI. Conclusion and Future Work

This paper introduced the new concept of Hybrid Cable-Thruster-actuated UVMS. The kinematic and dynamic modeling was presented. Then, we proposed a characterization of the available end-effector force set. This characterization allows to directly verify whether or not a given desired end-effector force is feasible. As an illustrative example, the case study of a planar HCT-actuated UVMS has been presented. A prototype of an HCT-actuated UVMS with four actuation cables and six thrusters is currently under development at LIRMM and should be available soon to validate the concepts introduced in this paper.

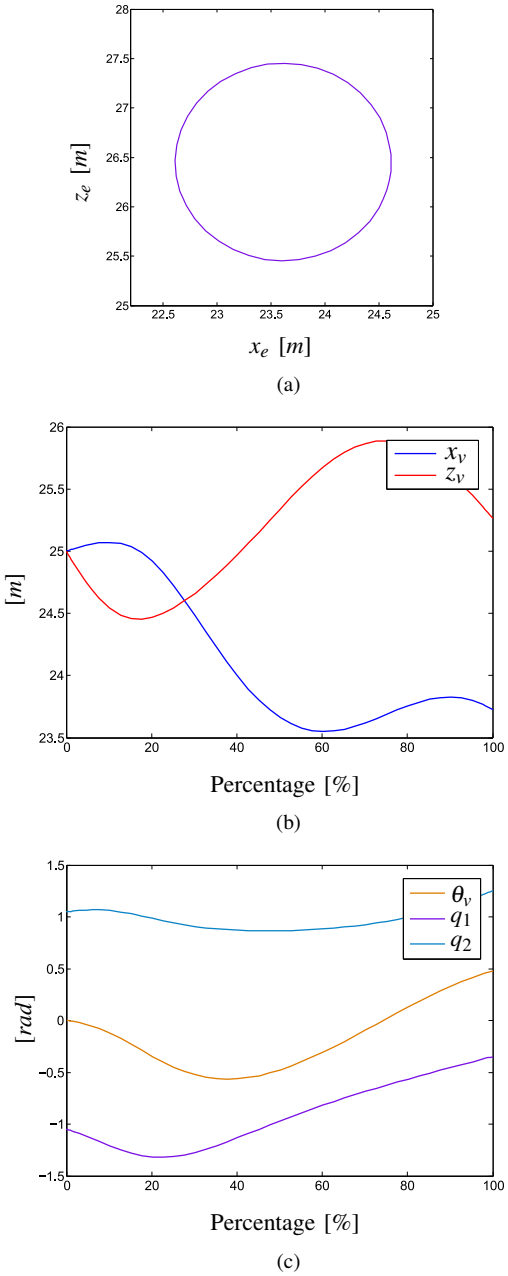

Fig. 8: Desired path. (a) Path in task space. (b) Path in configuration space (translational DOFs). (c) Path in configuration space (rotational DOFs).

References

[1] G. Antonelli, T. I. Fossen, and D. Yoerger, "Underwater Robotics," in *Springer Handbook of Robotics* (B. Siciliano and O. Khatib, eds.), pp. 987–1008, Springer Berlin Heidelberg, 2008.

[2] P. Ridao, M. Carreras, D. Ribas, P. J. Sanz, and G. Oliver, "Intervention AUVs: The next challenge," in *Proceeding of 19th IFAC World Congress*, pp. 12146–12159, Aug 2014.

[3] M. Prats, D. Ribas, N. Palomeras, J. C. García, V. Nannen, S. Wirth, J. J. Fernández, J. P. Beltrán, R. Campos, P. Ridao, P. J. Sanz, G. Oliver, M. Carreras, N. Gracias, R. Marín, and A. Ortiz, "Reconfigurable AUV for intervention missions: a case study on underwater object recovery," *Intelligent Service Robotics*, vol. 5, no. 1, pp. 19–31, 2012.

[4] D. Ribas, N. Palomeras, P. Ridao, M. Carreras, and A. Mallios, "Girona 500 AUV: From survey to intervention," *Mechatronics, IEEE/ASME Transactions on*, vol. 17, pp. 46–53, Feb 2012.

[5] H. Chen, S. Stavinoha, M. Walker, B. Zhang, and T. Fuhlbrigge, "Opportunities and challenges of robotics and automation in offshore oil gas industry," *Intelligent Control and Automation*, vol. 5, no. 5, pp. 136–145, 2014.

[6] T. Bruckmann, L. Mikelsons, T. Brandt, M. Hiller, and D. Schramm, "Wire robots Part I: Kinematics, analysis and design," in *Parallel Manipulators, New Developments* (J.-H. Ryu, ed.), pp. 109–132, InTech, 2008.

[7] T. Bruckmann, L. Mikelsons, T. Brandt, M. Hiller, and D. Schramm, "Wire robots Part II: Dynamics, control and application," in *Parallel Manipulators, New Developments* (J.-H. Ryu, ed.), pp. 133–152, InTech, 2008.

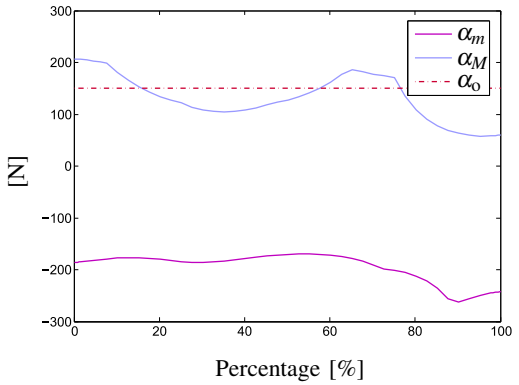

(a)

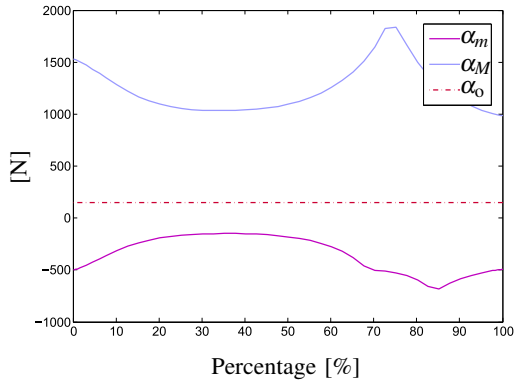

(b)

Fig. 9: Evolution of α_m and α_M at $\boldsymbol{s} = [0, -1]^T$. (a) Cable-free UVMS. (b) HCT-actuated UVMS.

[8] M. Carricato and J.-P. Merlet, "Geometrico-static analysis of under-constrained cable-driven parallel robots," in *Advances in Robot Kinematics: Motion in Man and Machine* (J. Lenarcic and M. M. Stanisic, eds.), pp. 309–319, Springer Netherlands, 2010.

[9] J. Albus, R. Bostelman, and N. Dagalakis, "The NIST robocrane," *Journal of Robotic Systems*, vol. 10, no. 5, pp. 709–724, 1993.

[10] S. Chiaverini, G. Oriolo, and I. D. Walker, "Kinematically redundant manipulators," in *Springer Handbook of Robotics* (B. Siciliano and O. Khatib, eds.), pp. 245–268, Springer Berlin Heidelberg, 2008.

[11] E. Olguín-Díaz, *Modélisation et commande d'un système véhcule/manipulateur sous marin*. PhD thesis, Laboratoire d'Automatique de Grenoble, Institut National Polytechnique de Grenoble, Grenoble, France, 1999.

[12] G. Antonelli, *Underwater Robots - 2nd Edition - Motion and Force Control of Vehicle-Manipulator Systems*, vol. 2 of *Springer Tracts in Advanced Robotics*. Springer, 2006.

[13] I. Schjølberg and T. I. Fossen, "Modelling and control of underwater vehicle-manipulator systems," in *Proceeding of Third IFAC Conference on Marine Craft Maneuvering and Control*, pp. 45–57, 1994.

[14] T. I. Fossen, *Guidance and control of ocean vehicles*. John Wiley & Sons, Ltd, 1994.

[15] T. I. Fossen, *Marine control systems: guidance, navigation and control of ships, rigs and underwater vehicles*. Marine Cybernetics AS, 2002.

[16] T. I. Fossen, *Handbook of marine craft hydrodynamics and motion control*. John Wiley & Sons, Ltd, 2011.

[17] C. Gosselin, "Cable-driven parallel mechanisms: state of the art and perspectives," *Mechanical Engineering Reviews*, vol. 1, no. 1, pp. DSM0004–DSM0004, 2014.

[18] J. Lamaury and M. Gouttefarde, "A tension distribution method with improved computational efficiency," in *Cable-driven parallel robots*, pp. 71–85, Springer, 2013.

[19] F. Guay, P. Cardou, A. L. Cruz-Ruiz, and S. Caro, "Measuring how well a structure supports varying external wrenches," in *New Advances in Mechanisms, Transmissions and Applications* (V. Petuya, C. Pinto, and E.-C. Lovasz, eds.), vol. 17 of *Mechanisms and Machine Science*, pp. 385–392, Springer Netherlands, 2014.

[20] S. Bouchard, C. Gosselin, and B. Moore, "On the ability of a cable-driven robot to generate a prescribed set of wrenches," *Journal of Mechanisms and Robotics*, vol. 2, no. 1, p. 011010, 2010.

[21] M. Gouttefarde and S. Krut, "Characterization of parallel manipulator available wrench set facets," in *Advances in Robot Kinematics: Motion in Man and Machine* (J. Lenarcic and M. M. Stanisic, eds.), pp. 475–482, Springer Netherlands, 2010.

[22] P. Chiacchio, Y. Bouffard-Vercelli, and F. Pierrot, "Force polytope and force ellipsoid for redundant manipulators," *Journal of Robotic Systems*, vol. 14, no. 8, pp. 613–620, 1997.